Supporting information

for

Single-crystalline Ni(OH)$_2$ nanosheets vertically aligned on three-dimensional nanoporous metal for high-performance asymmetric supercapacitors

Chao Hou, Xing-You Lang*, Zi Wen, Yong-Fu Zhu, Ming Zhao, Jian-Chen Li, Wei-Tao Zheng, Jian-She Lian, Qing Jiang*

Key Laboratory of Automobile Materials (Jilin University), Ministry of Education,

and School of Materials Science and Engineering, Jilin University, Changchun

130022, China

* Correspondence and requests for materials should be addressed to X.Y.L. (email: xylang@jlu.edu.cn) or Q.J. (email: jiangq@jlu.edu.cn).
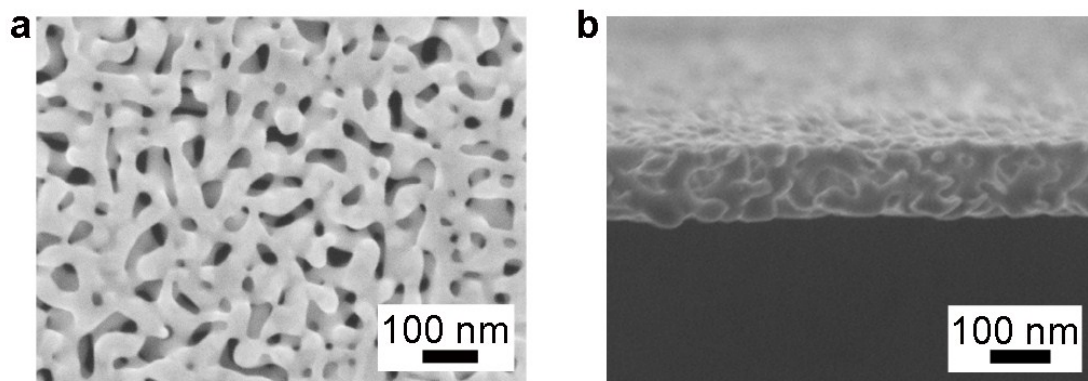
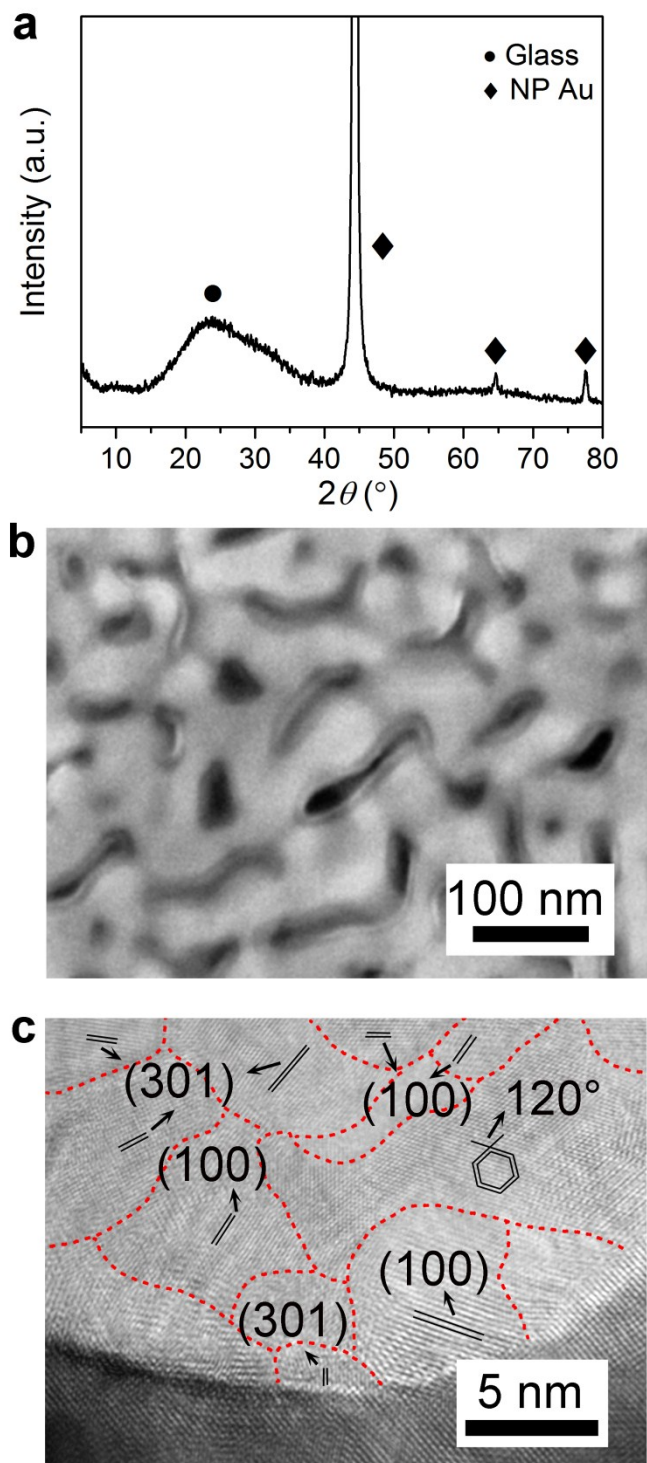**Figure S1**. SEM images of **(a)** top view and **(b)** cross-sectional view of NP Au.

Figure S2. **(a)** XRD pattern **(b)** SEM and **(c)** HRTEM image of NP Au/RA Ni(OH)$_2$ electrode fabricated without the addition of K$_2$S$_2$O$_8$ in the aqueous solution.
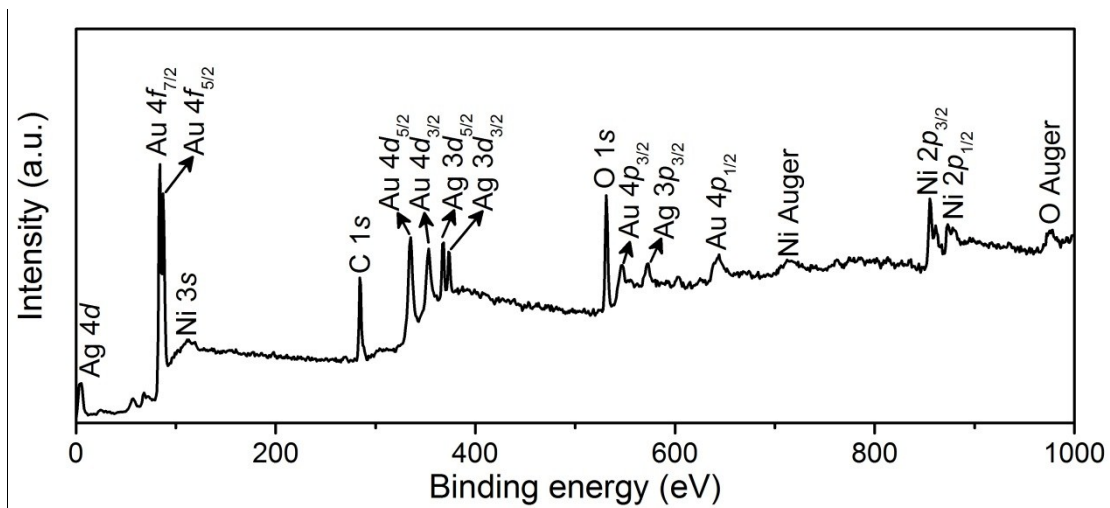
Figure S3. Typical XPS survey spectrum for the NP Au/VA Ni(OH)$_2$ electrode.
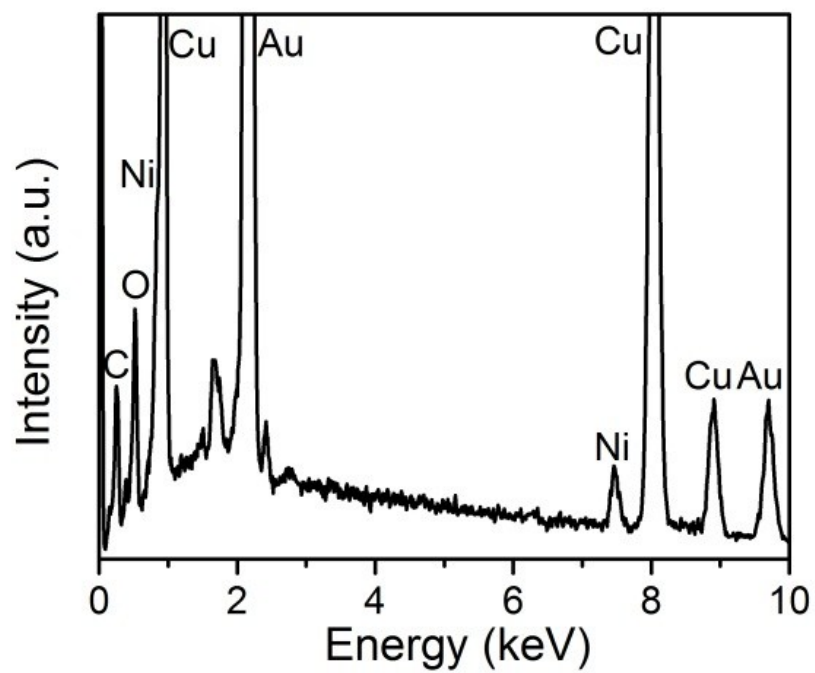
Figure S4. EDS spectrum of NP Au/VA Ni(OH)$_2$ electrode. The content Cu was from supported Cu foil.
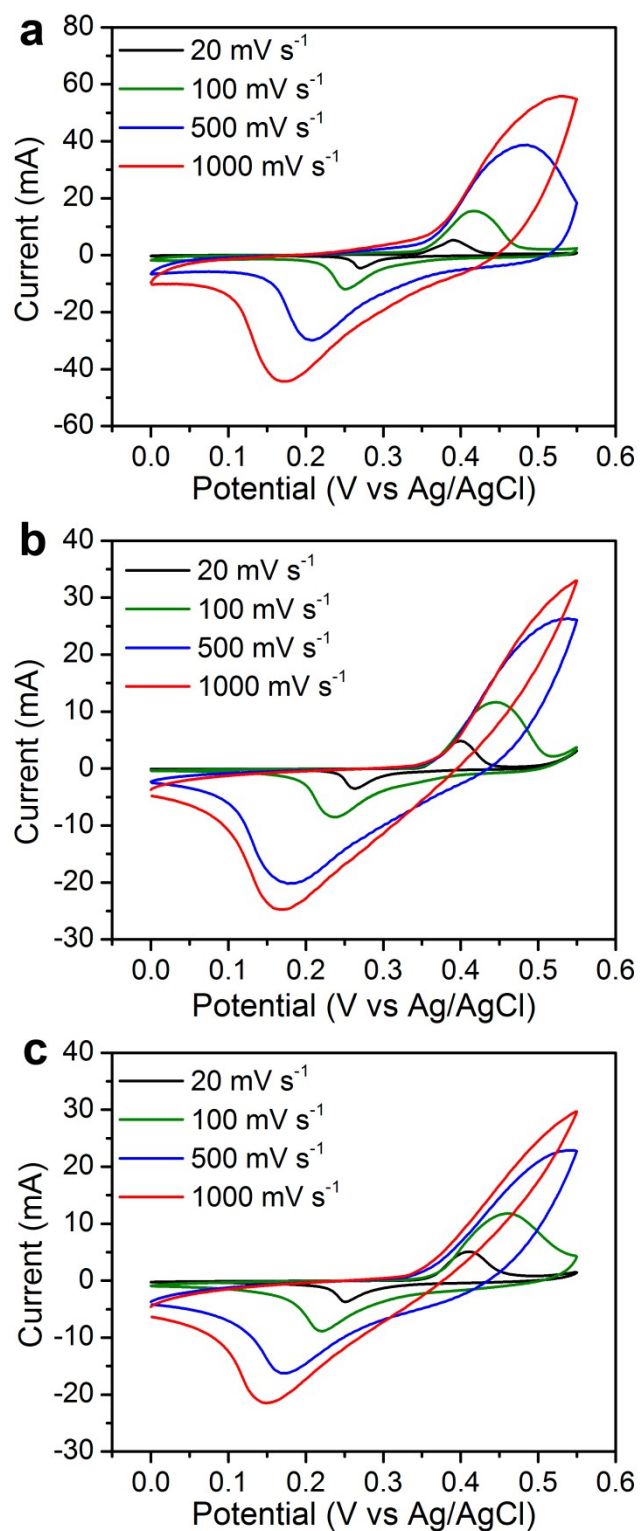
Figure S5. Typical CV curves of **(a)** NP Au/RA Ni(OH)$_2$,. **(b)** CFP/VA Ni(OH)$_2$ and **(c)** CFP/RA Ni(OH)$_2$ electrodes at various scan rates.
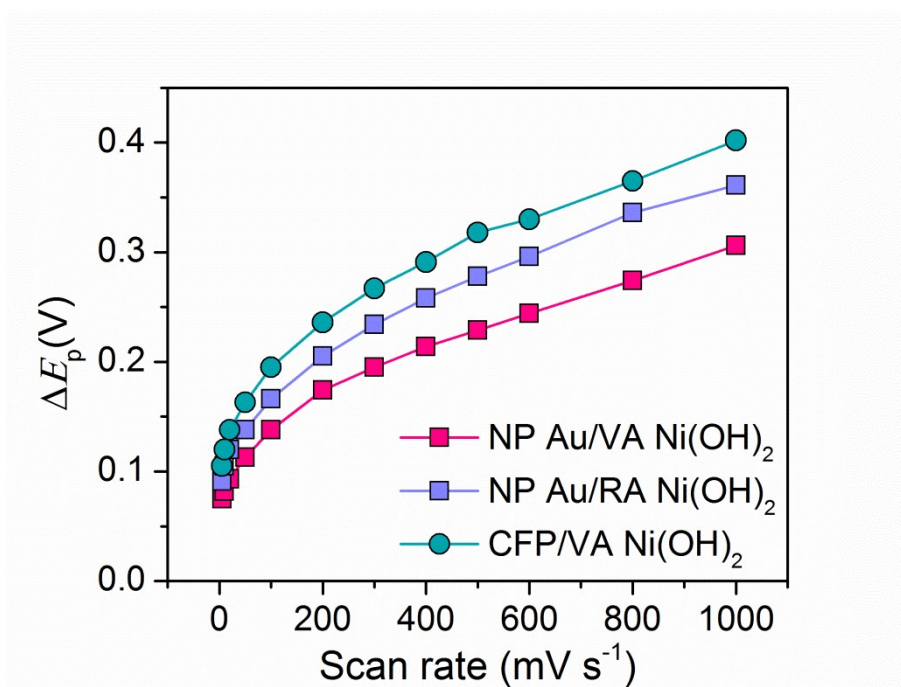
Figure S6. The potential difference between the anodic peaks and the cathode peaks ($\Delta E_p = E_O\text{-}E_R$) for NP Au/VA Ni(OH)$_2$, NP Au/RA Ni(OH)$_2$ and CFP/VA Ni(OH)$_2$ electrodes as a function of scan rate.
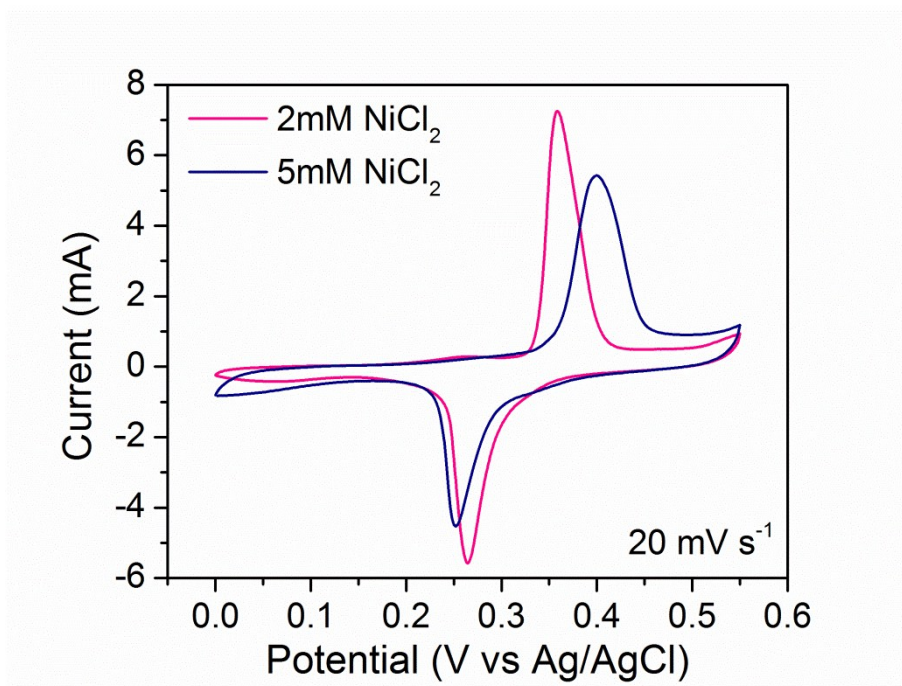
Figure S7. Comparison of CV curves for NP Au/VA Ni(OH)$_2$ with different loading of Ni(OH)$_2$, which is controlled by using different concentration of precursor NiCl$_2$. The scan rate is 20 mV s^{-1}.
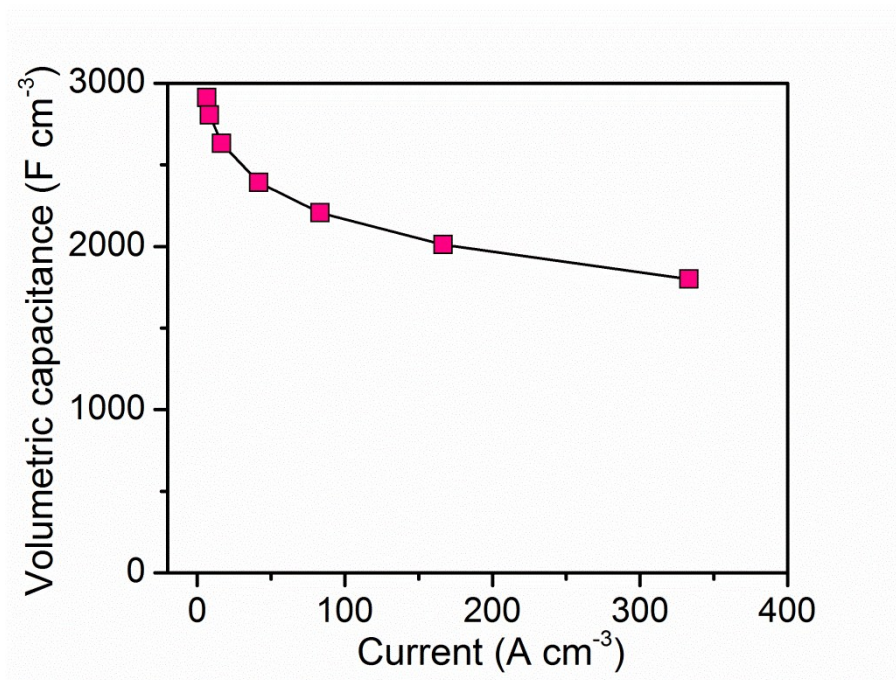
Figure S8. Volumetric capacitance of NP Au/VA Ni(OH)$_2$ electrode as a function of volumetric current density.
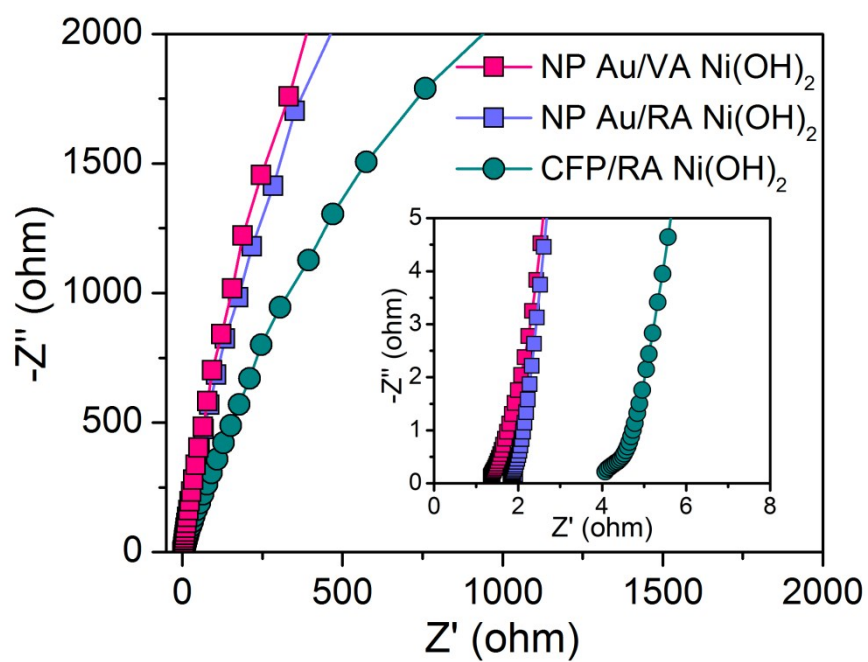
Figure S9. Complex plane plot of the impedances of NP Au/VA Ni(OH)$_2$, NP Au/RA Ni(OH)$_2$ and CFP/VA Ni(OH)$_2$ electrodes, with a magnification for the high frequency region in the inset.
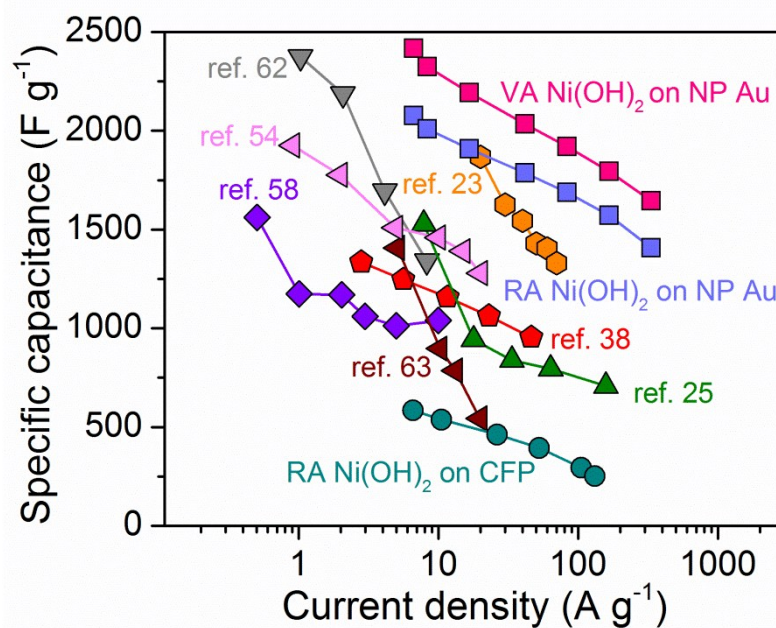
Figure S10. Specific capacitance of constituent VA Ni(OH)$_2$ on NP Au, in comparison with RA Ni(OH)$_2$ on NP Au, RA Ni(OH)$_2$ on CFP and other previously reported Ni(OH)$_2$-based electrodes, such as graphite/amorphous Ni(OH)$_2$,[23] Ni foil/3D Ni(OH)$_2$,[25] graphene/Ni(OH)$_2$,[38] Au nanoparticles-deposited Ni(OH)$_2$,[54] 3D graphite foam/Ni(OH)$_2$,[58] Ni foam/CoO/Ni(OH)$_2$,[62] and 3D graphene/Ni$_3$S$_2$/Ni(OH)$_2$ electrodes.[63]
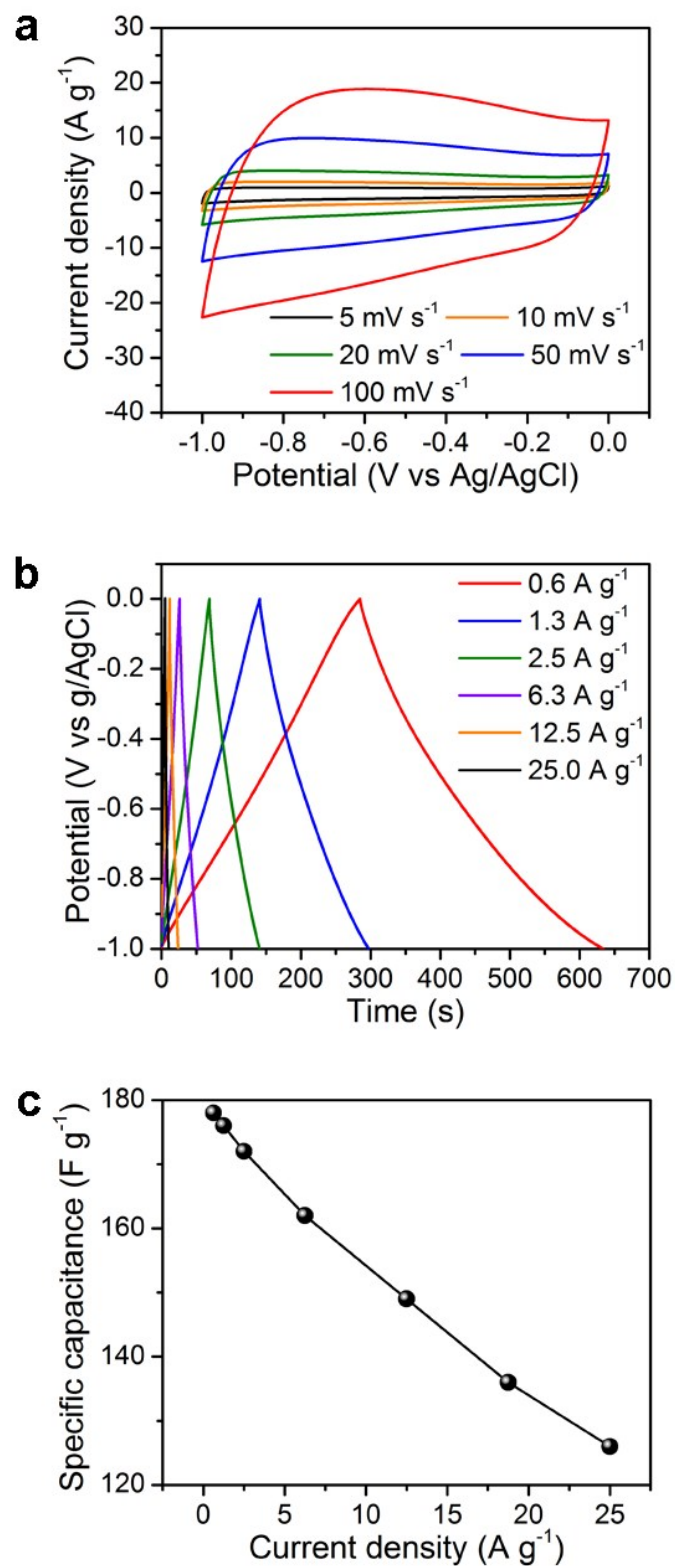
Figure S11. Electrochemical performance of AC electrode. **(a)** CV curves, **(b)** charge/discharge profiles and **(c)** specific capacitance of the AC electrode derived from discharge curves.
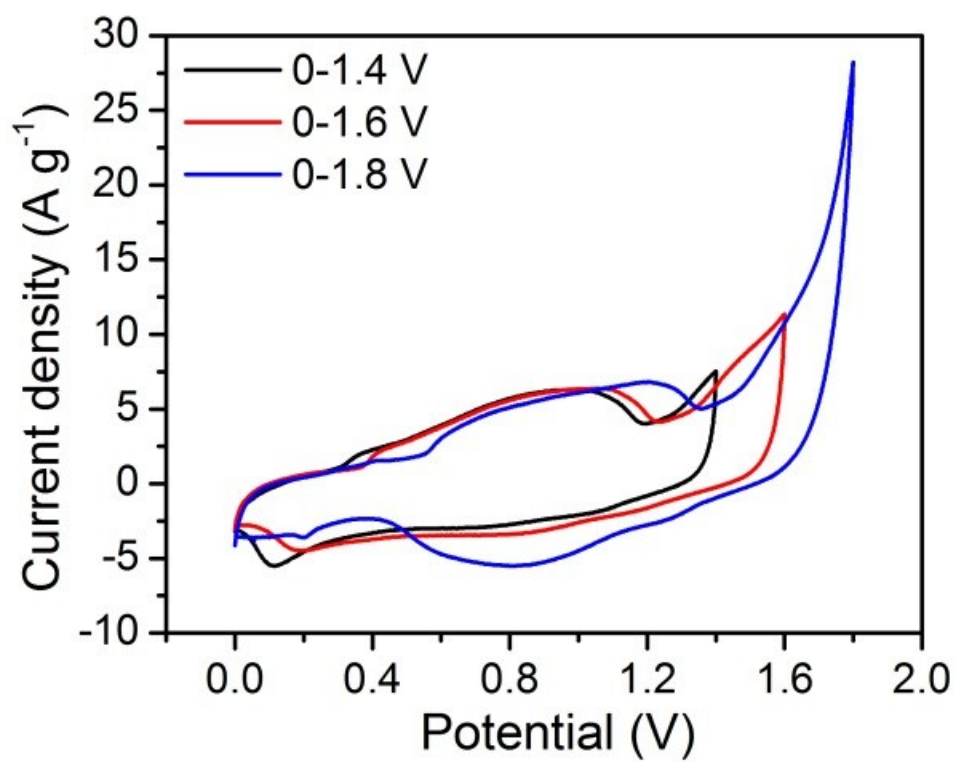
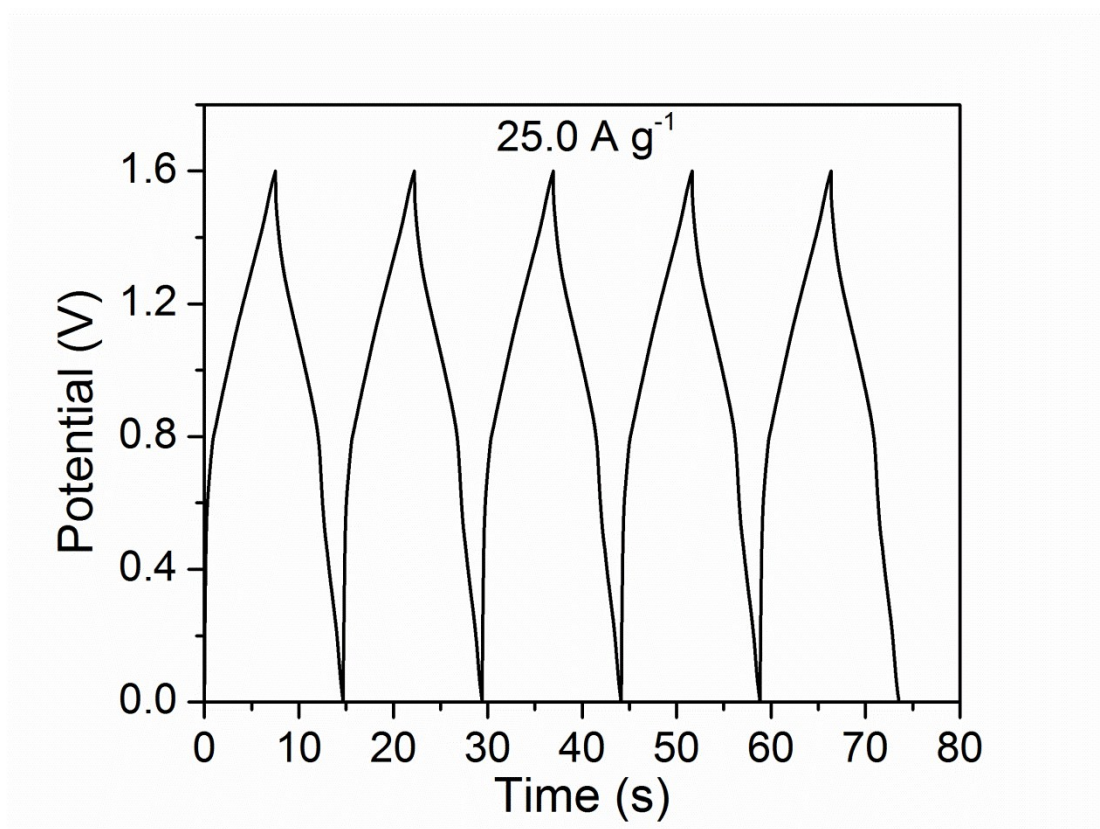**Figure S12**. CV curves of ASC device at various potential windows at 20 mV s^{-1}.

Figure S13. Charge-discharge curves of ASC device at a current density of 25.0 A g^{-1}.
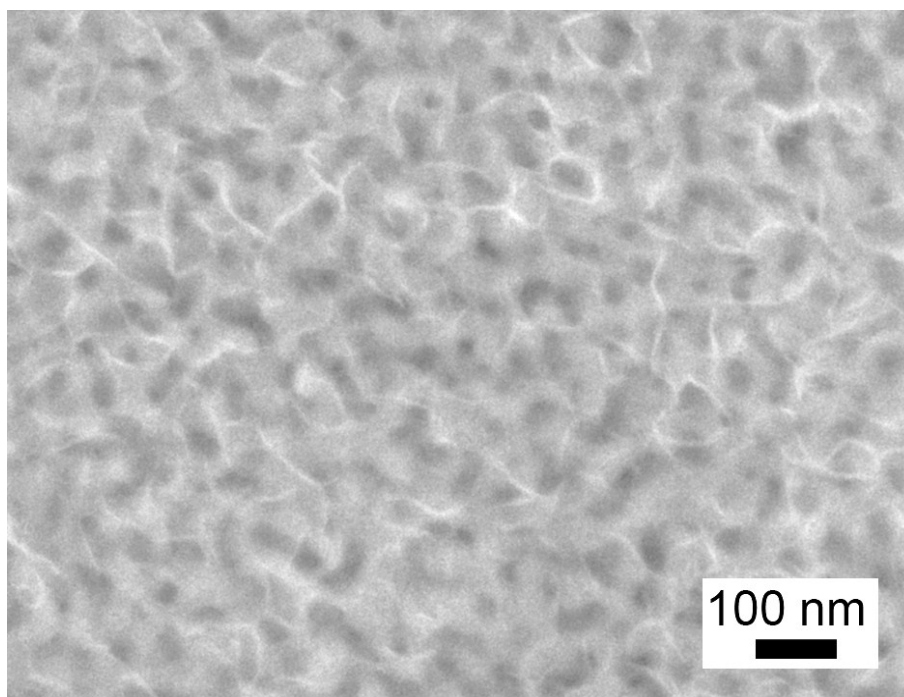
Figure S14. SEM image of NP Au/VA Ni(OH)$_2$ after the stability test of 10000 cycles.